Breaking a Dative Bond with Mechanical Forces

Pengcheng Chen
Princeton University
Dingxin Fan
Purdue University West Lafayette
Yunlong Zhang
ExxonMobil (United States)
Annabella Selloni
Department of Chemistry, Princeton University, Princeton, New Jersey 08544 https://orcid.org/0000-0001-5896-3158
Emily Carter
University of California Los Angeles https://orcid.org/0000-0001-7330-7554
Craig Arnold
Princeton University
David Dankworth
ExxonMobil (United States) https://orcid.org/0000-0003-4674-9407
Steven Rucker
ExxonMobil (United States) https://orcid.org/0000-0003-2619-6278
James Chelikowsky
University of Texas https://orcid.org/0000-0003-2181-3070
Nan Yao (nyao@princeton.edu)
Princeton University https://orcid.org/0000-0002-4081-1495

Article

Keywords: chemical bond breaking, chemical bond forming, dative bond

Posted Date: March 16th, 2021

DOI: https://doi.org/10.21203/rs.3.rs-299820/v1

Version of Record: A version of this preprint was published at Nature Communications on September 24th, 2021. See the published version at https://doi.org/10.1038/s41467-021-25932-6.

Abstract

Bond breaking and forming is essential in every chemical reaction. Here, we report a single dative bond breaking process revealing an unprecedented level of detail using noncontact atomic force microscopy. The dative bond between carbon monoxide and ferrous phthalocyanine was ruptured via mechanical forces applied by atomic force microscope tips; the process was quantitatively measured and characterized both experimentally and via first principles quantum mechanics modeling. Our results show that the bond can be ruptured either by applying an attractive force of ~150 pN (pulling) or by a repulsive force of ~220 pN (pushing), accompanied by changes of the spin state of the system. Our combined experimental and computational studies provide a deeper understanding of the chemical bond breaking process.

Introduction

The ability to obtain the direct image of organic molecules with subatomic resolution was first demonstrated by Gross *et al*. in 2009 by using a carbon monoxide (CO) molecule attached to an Atomic Force Microscope (AFM) tip[1] mounted on a qPlus sensor[2]. This work inspired a wide range of applications, including directly characterizing molecular structures[3,4,5], probing molecular properties[6-10], creating new structures[11,12], and even providing afor studying various types of chemical bonds, such as hydrogen bonds and halogen bonds[13,14]. These studies stimulated significant discussions on the contrast mechanism of AFM images and on the extent to which the image could represent a physical description of a chemical bond[15,16]. Recently, this technique also has been used to directly manipulate individual chemical bonds. For example, Kawai *et al.* designed a system to study a hydrogen bond with a direct measurement of bond strength[17], and Huber, *et al.* reported the bond-forming process and the transition from physisorption to chemisorption[18].

Besides bond formation, the controlled breaking of a chemical bond using mechanical forces, along with accurate measurements of these forces, is also important and has not yet been achieved. It is essential for better understanding the physical nature of a chemical bond. Here we focus on understanding the breaking of a single dative bond between a CO molecule and a ferrous phthalocyanine (FePc) complex. Dative bonds involve an electron pair on one molecule delocalizing into an empty orbital on an acceptor atom or molecule. They are quite common especially in transition-metal complexes and play vital roles in the fields of catalysis, organometallic chemistry, and biochemistry. Dative bonds have been investigated extensively via ensemble measurements, e.g., X-ray photoelectron spectroscopy, X-ray crystallography, and infrared and Raman spectroscopy[19,20]. Recently, electrochemically controlled AFM was also employed to investigate the force required to break the bond between osmium ions and pyridine ligands[21]. While providing useful insights, that study was carried out in a liquid environment and the observed reaction involved a ligand substitution process, as opposed to a pure ligand dissociation process. Here, we report the realization of a system containing an individual CO and FePc and subsequent AFM studies of the bond rupture process under vacuum conditions, so as to minimize the

effects of environmental perturbations. Together with real-space pseudopotential density functional theory (DFT) calculations[22-24] modeling the events, this work advances our understanding of the origins of the measured forces in dative bond breaking.

Results

A supported CO-FePc system was prepared by dosing CO molecules onto FePc adsorbed on a Cu (111) surface at 4.8 K. The scanning tunneling microscope (STM) image in Figure 1a shows two distinct features for the FePc molecule and the complex (CO-FePc), which are similar to previously reported STM images on other surfaces[25]. AFM images were obtained using a CO-terminated tip, confirming their respective structures (Figures 1b and c). The AFM image in Figure 1b of the CO-FePc complex featured a protruding center due to the CO attached to Fe. This was confirmed by comparing with AFM images of FePc molecules on the surface (1c), and further verified by our simulated images (Figures 1d and e).

The dative CO-FePc bond is known to be formed via σ-donation from the CO 5σ orbital and π-back donation from Fe dπ[26-29]. We studied the rupture of this dative bond by applying mechanical forces using the scanning tip of the AFM. The same CO-terminated tip employed for imaging was used first because it is known to be chemically inert[1]. By decreasing the tip height, the repulsive interactions increased, as indicated by the increased contrast in the images (Figure 2a (ii-iv)). At a lower tip height (+40 pm), the peripheral aromatic rings of FePc became visible, while the center of the image became distorted due to strong repulsions with the tip. Upon further reducing the tip height (+30 pm), a sudden change of the image occurred during scanning, as indicated by a line created with a different contrast. Subsequent scans showed the repulsion had disappeared, indicating that the CO attached to FePc was dislodged due to the strong repulsion with the tip. The chemical structure of FePc revealed from subsequent scanning of the lower part of the molecule confirmed that a free FePc was left after CO removal and that the tip remained intact during the dissociation. Comparison of the contrast in the lower part to the upper part of the same AFM image (**iv**) obtained at the same tip height reveals a downward shift of FePc by ~ 30 pm upon CO removal. This shift is likely due to the *trans* effect by the Cu substrate on the FePc complex[26-30], whereby the binding or removal of one ligand respectively reduces or enhances the strength of the bond to the ligand on the opposite side[31]. This observation confirmed the rupture of the dative bond between CO and FePc induced by the increased interactions during tip scanning.

To elucidate the CO-FePc bond rupture, we performed detailed measurements of the interaction forces during the entire bond rupture process. Figure 2b shows a 3D force map representing the original frequency shift (Δf) obtained at different tip heights (z) by scanning across the center of the CO-FePc complex (shown in the insert). The dislodging of the CO was indicated by a break point (x = 0) with decreasing the tip height during scanning and by the discontinuity in the frequency shift (Δf) curve (red curve in Fig. 2c). The deconvoluted force curve along the tip height (z) at the breaking point (x = 0), in Fig. 2d, shows that the dative bond ruptured with a force of 220±30 pN, after passing a maximal force at ~300 pN.

Dislodging experiments were also performed with a bare metal tip terminated by a Cu atom under similar experimental conditions as using the CO-terminated tip. The Cu atom tip is known to be a chemically active tip[1]. When the Cu-tip was used, only attractive interactions between the tip and CO-FePc were detected (Figure 2e), until the rupture of the dative bond took place. At this point, the attractive force reached 150±30 pN by reducing the tip height (Figures 2f, g).

The observation that both a repulsive force of +220 pN and an attractive force of -150 pN are capable of breaking the same dative bond indicates the important role of the probe tip. It is difficult to rationalize how a compressive force could break a chemical bond as the single bond strength is often correlated with the bond length,[32] unless it is through a displacement. We performed real-space DFT calculations to address these questions to and shed light on the details of the bond-breaking process. Both model tips were initially positioned at relatively large heights (~500 pm) to compute the relative frequency shifts using a finite difference method[26]. The calculated frequency shift curves (scaled) for both tips agreed very well with the measurements (dashed curves in Figures 2c and 2f).

Due to the multidimensional interactions between the two CO molecules for the CO-tip (*vide infra*), the Cu-tip is examined first (Figure 3a). The calculated maximum force (-156 pN) at the Cu tip apex agrees closely with the measured force of -150±30 pN (Figure 3b). Furthermore, as the force on the tip apex approaches a maximum at a Fe-C bond distance of ~1.9-2.1 Å (shaded area), a low spin to high spin transition of the system occurs (Figure 3b). The change in spin states suggests the breaking of the dative bond, as demonstrated by a previous DFT study of the CO-FePc complex on a Au(111) surface[31]. For a CO-tip, simply applying a compressive vertical force from above the CO-FePc was not sufficient to break the bond. Therefore, we simulated the experimental process where the tip approaches the CO-FePc complex horizontally (Figure 3c), similar to the AFM scanning along the x direction (see Supplementary Materials for the equilibrium geometry). Using this method, while a small increase of the vertical force acting on the tip apex was observed (Figure 3d), a lateral force emerged at the same time acting on the C attached to FePc and rapidly increased to a few nN (Figure 3e). High resolution calculations (dashed curves inside the red boxes) indicate the bond was likely broken when the shear force approaches ~400 pN on the bottom C atom of the CO-FePc complex. Bond rupture by a shear force of 400 pN is reasonable given the fact that the Fe-C dative bond is weaker than typical single bonds[21]. Therefore, our calculations confirm that the lateral force is most likely responsible for the breaking of the dative bond when the compressive force (220 pN) was applied by the CO-terminated tip.

The calculated spin-polarized local density of states (LDOS) projected onto the center Fe atom of the system shows that the removal of CO results in an increase (from 0.00 to 1.20 μ_B) in the net magnetic moment (Figures 4a and b). This change in spin state is consistent with Figure 3b and a previous DFT study of the CO-FePc complex on the Au(111) surface[31]. The total electron density and the highest occupied molecular orbital (HOMO) of the CO-FePc system demonstrate that the Fe center interacts with the two bridge Cu atoms underneath via the d_{z^2} orbital (Figures 4a and d). Figures 4a and c show the

presence of the Cu(111) substrate weakens the Fe-C dative bond by shifting the d_z^2 orbital toward the HOMO. These results confirm the rupture of the dative bond.

Discussion And Conclusion

Our study shows that the dative bond in the CO-FePc complex can be broken by mechanical forces imposed by AFM tips. DFT calculations reveal that the measured forces correspond to the net forces applied at the tip apex, and confirm the directions and magnitudes of the applied forces for both tips. While a direct vertical attractive force is responsible for the bond rupture in the case of a Cu-tip, the bond rupture is more likely caused by a lateral repulsive force in the case of a CO-tip. Our calculations also show that although the dative CO-FePc bond is weakened by the presence of the Cu(111) substrate[18,21], the ruptured bond is indeed a chemical, rather than a physical bond[18], as indicated by the computed Fe-C bond length of ~1.7 Å. The Cu-Fe interaction is strengthened and shortened from 2.73 Å to 2.48 Å upon CO removal, consistent with the downward shift of FePc by ~30 pm observed during dislodging of the CO by the AFM tip.

Our combined experimental and theoretical results shed detailed new insights into the CO-FePc bond breaking process. When the bond is ruptured by the Cu tip, the σ donation from CO to Fe is weakened by the tip Cu atoms. On the other hand, when the bond is broken with a CO-terminated tip, the two CO molecules repel each other (due to Pauli repulsion) and the dative bond of CO-FePc is tilted by the lateral force. This tilting is required for the rupture of the bond, but unfavorable due to the symmetry of σ donation, which is consistent with the higher force before the bond breaking that is observed in the experiment. This detailed information on the rupture of the bond between CO and FePc could help to better understand other dative bonds, such as CO-heme interactions in biochemistry[26,33], as well as chemical reactions of materials under mechanical stress[19,34].

Materials And Methods

The experiments were performed with a CreaTec^{TM} STM/AFM system under ultrahigh vacuum (UHV) conditions of ~10^{-10} mbar and a temperature of approximately 5 K. The qPlus sensor has a resonance frequency of 30 kHz with a spring constant k = 1,800 N/m. In our measurements, the quality factor of the sensor is about 20,000. To minimize the crosstalk between the qPlus signal and the STM channel, no voltage was applied on the tip during the force measurement process. The oscillation amplitude was set to be 100 pm. The iron(II) phthalocyanine (FePc, dye content ~90%, Sigma-Aldrich) molecules were evaporated from a silicon chip via direct heating and the vapor was subsequently deposited on a Cu(111) substrate held at 5 K. The AFM Cu-tip apex can be functionalized by controlled pickup of a CO molecule from the substrate[1]. All the experiments were conducted using a pure Cu tip or a CO-functionalized tip.

We computed ground state energies using a real-space pseudopotential DFT code, PARSEC[35]. We employed the local density approximation (LDA) by Perdew-Wang (PW92)[36] for the exchange-correlation

functional together with Troullier-Martins norm-conserving pseudopotentials[37]. We also tested another LDA exchange-correlation functional by Ceperley-Alder[38]; the differences were negligible. In addition, a previous study showed that LDA and the generalized gradient approximation (GGA) gave similar results for properties of FePc and CO-FePc on Au(111)[31]. We assumed the electron wave functions to vanish outside a spherical or a slab domain. We set the distance between neighbor points in the real-space grid to be 16 pm. The density-weighted self-consistent residual error was less than 10^{-4} Ry. We employed a finite difference method to approximate the relative frequency shift profiles based on the computed ground state energies across the middle line of the FePc complex, as indicated in Figures 2c and f at relatively large tip heights. We performed further structural relaxations when the tips were close to the specimen, as the assumption that the movement of the tip had negligible influence on the electronic structure of the specimen became invalid. We then applied the Hellmann-Feynman theorem to the total ground state energies to compute the net forces acting on each atom. For the AFM image simulations, we used the same method as described in Ref [24]. (See Supplementary Materials for more details.)

Declarations

Acknowledgements:

General: The authors gratefully acknowledge Yeju Zhou, Dan Gregory, and Guangming Cheng for help with data processing and general discussion.

Funding: This work was supported by ExxonMobil through its membership in the Princeton E-filliates Partnership of the Andlinger Center for Energy and the Environment. This research made use of the Imaging and Analysis Center operated by the Princeton Institute for the Science and Technology of Materials at Princeton University, which is supported in part by the Princeton Center for Complex Materials, a National Science Foundation Materials Research Science and Engineering Center (Grant No. DMR-2011750). D.F. and J.R.C. acknowledge support from the Welch Foundation under grant F-1837 and the U.S. Department of Energy under DOE/DE-FG02-06ER46286. The National Energy Research Scientific Computing (NERSC) and the Texas Advanced Computing Center (TACC) provided computational resources.

Author contributions: P.C. and N.Y. designed and carried out the experiments. D.F. and J.R.C. performed the DFT calculations. A.S. and E.A.C. provided theoretical insight. P.C., N.Y., Y.Z., D.F., drafted the manuscript with the input from A.S., J.R.C., E.A.C., C.B.A., D.C.D, and S.P.R. N.Y. directed the project. All authors discussed the results, contributed to the interpretation and conclusion. Competing interests: The authors declare no competing interests. Data and materials availability: All data are available in the main text or the supplementary materials.

References

1. Gross, L., Mohn, F., Moll, N., Liljeroth, P. & Meyer, G. The Chemical Structure of a Molecule Resolved by Atomic Force Microscopy. *Science* **325,** 1110 LP-1114 (2009).
2. Giessibl, F. J. High-speed force sensor for force microscopy and profilometry utilizing a quartz tuning fork. *Appl. Phys. Lett.* **73,** 3956–3958 (1998).
3. Gross, L. *et al.* Organic structure determination using atomic-resolution scanning probe microscopy. *Nat. Chem.* **2,** 821–825 (2010).
4. Schuler, B. *et al.* Heavy Oil Based Mixtures of Different Origins and Treatments Studied by Atomic Force Microscopy. *Energy & Fuels* **31,** 6856–6861 (2017).
5. Hanssen, K. Ø. *et al.* A Combined Atomic Force Microscopy and Computational Approach for the Structural Elucidation of Breitfussin A and B: Highly Modified Halogenated Dipeptides from Thuiaria breitfussi. *Angew. Chemie Int. Ed.* **51,** 12238–12241 (2012).
6. Gross, L. *et al.* Bond-Order Discrimination by Atomic Force Microscopy. *Science* **337,** 1326–1329 (2012).
7. Fatayer, S. *et al.* Molecular structure elucidation with charge-state control. *Science* **365,** 142–145 (2019).
8. Gross, L. *et al.* Measuring the Charge State of an Adatom with Noncontact Atomic Force Microscopy. *Science* **324,** 1428–1431 (2009).
9. Mohn, F., Gross, L., Moll, N. & Meyer, G. Imaging the charge distribution within a single molecule. *Nat. Nanotechnol.* **7,** 227–231 (2012).
10. de Oteyza, D. G. *et al.* Noncovalent Dimerization after Enediyne Cyclization on Au(111). *J. Am. Chem. Soc.* **138,** 10963–10967 (2016).
11. Pavliček, N. *et al.* Synthesis and characterization of triangulene. *Nat. Nanotechnol.* **12,** 308–311 (2017).
12. Kaiser, K. *et al.* An sp-hybridized molecular carbon allotrope, cyclo[18]carbon. *Science* **365,** 1299–1301 (2019).
13. Zhang, J. *et al.* Real-Space Identification of Intermolecular Bonding with Atomic Force Microscopy. *Science* **342,** 611 LP-614 (2013).
14. Han, Z. *et al.* Imaging the halogen bond in self-assembled halogenbenzenes on silver. *Science* **358,** 206 LP-210 (2017).
15. Ellner, M., Pou, P. & Pérez, R. Molecular Identification, Bond Order Discrimination, and Apparent Intermolecular Features in Atomic Force Microscopy Studied with a Charge Density Based Method. *ACS Nano* **13,** 786–795 (2019).
16. Hämäläinen, S. K. *et al.* Intermolecular Contrast in Atomic Force Microscopy Images without Intermolecular Bonds. *Phys. Rev. Lett.* **113,** 186102 (2014).
17. Kawai, S. *et al.* Direct quantitative measurement of the C=O...H-C bond by atomic force microscopy. *Sci. Adv.* **3,** (2017).

18. Huber, F. *et al.* Chemical bond formation showing a transition from physisorption to chemisorption. *Science* **366,** 235 LP-238 (2019).
19. Boucly, A. *et al.* Soft X-ray Heterogeneous Radiolysis of Pyridine in the Presence of Hydrated Strontium-Hydroxyhectorite and its Monitoring by Near-Ambient Pressure Photoelectron Spectroscopy. *Sci. Rep.* **8,** 6164 (2018).
20. Świderski, G. *et al.* Thermal, spectroscopic, X-ray and theoretical studies of metal complexes (sodium, manganese, copper, nickel, cobalt and zinc) with pyrimidine-5-carboxylic and pyrimidine-2-carboxylic acids. *J. Therm. Anal. Calorim.* **138,** 2813–2837 (2019).
21. Hao, X. *et al.* Direct measurement and modulation of single-molecule coordinative bonding forces in a transition metal complex. *Nat. Commun.* **4,** 2121 (2013).
22. Sakai, Y., Lee, A. J. & Chelikowsky, J. R. First-Principles Atomic Force Microscopy Image Simulations with Density Embedding Theory. *Nano Lett.* **16,** 3242–3246 (2016).
23. Chelikowsky, J. R., Fan, D., Lee, A. J. & Sakai, Y. Simulating noncontact atomic force microscopy images. *Phys. Rev. Mater.* **3,** 110302 (2019).
24. Fan, D., Sakai, Y. & Chelikowsky, J. R. Chemical and steric effects in simulating noncontact atomic force microscopy images of organic molecules on a Cu (111) substrate. *Phys. Rev. Mater.* **4,** 53802 (2020).
25. Tsukahara, N., Minamitani, E., Kim, Y., Kawai, M. & Takagi, N. Controlling orbital-selective Kondo effects in a single molecule through coordination chemistry. *J. Chem. Phys.* **141,** 54702 (2014).
26. Stynes, D. V & James, B. R. Kinetics and equilibriums for carbon monoxide binding to ferrous phthalocyanine complexes. *J. Am. Chem. Soc.* **96,** 2733–2738 (1974).
27. Calderazzo, F. *et al.* Synthesis and Moessbauer spectroscopic studies of carbonyl derivatives of (phthalocyaninato)iron(II). *Inorg. Chem.* **21,** 2302–2306 (1982).
28. Li, J., Noll, B. C., Schulz, C. E. & Scheidt, W. R. Comparison of Cyanide and Carbon Monoxide as Ligands in Iron(II) Porphyrinates. *Angew. Chemie Int. Ed.* **48,** 5010–5013 (2009).
29. Collman, J. P., Brauman, J. I. & Doxsee, K. M. Carbon monoxide binding to iron porphyrins. *Proc. Natl. Acad. Sci.* **76,** 6035–6039 (1979).
30. Hieringer, W. *et al.* The Surface Trans Effect: Influence of Axial Ligands on the Surface Chemical Bonds of Adsorbed Metalloporphyrins. *J. Am. Chem. Soc.* **133,** 6206–6222 (2011).
31. Isvoranu, C. *et al.* Comparison of the Carbonyl and Nitrosyl Complexes Formed by Adsorption of CO and NO on Monolayers of Iron Phthalocyanine on Au(111). *J. Phys. Chem. C* **115,** 24718–24727 (2011).
32. Pauling, L. The Nature of The Chemical Bond. Application of Results Obtained from the Quantum Mechanics and from a Theory of Paramagnetic Susceptibility to the Structure of Molecules. *J. Am. Chem. Soc.* **53**, 1367–1400 (1931).
33. Collman, J. P., Brauman, J. I., Halbert, T. R. & Suslick, K. S. Nature of O_2 and CO binding to metalloporphyrins and heme proteins. *Proc. Natl. Acad. Sci. U. S. A.* **73,** 3333–3337 (1976).

34. Caruso, M. M. *et al.* Mechanically-Induced Chemical Changes in Polymeric Materials. *Chem. Rev.* **109,** 5755–5798 (2009).
35. Liou, K.-H., Yang, C. & Chelikowsky, J. R. Scalable implementation of polynomial filtering for density functional theory calculation in PARSEC. *Comput. Phys. Commun.* **254,** 107330 (2020).
36. Perdew, J. P. & Wang, Y. Accurate and simple analytic representation of the electron-gas correlation energy. *Phys. Rev. B* **45,** 13244–13249 (1992).
37. Troullier, N. & Martins, J. L. Efficient pseudopotentials for plane-wave calculations. *Phys. Rev. B* **43,** 1993–2006 (1991).
38. Ceperley, D. M. & Alder, B. J. Ground state of the electron gas by a stochastic method. *Phys. Rev. Lett.* **45,** 566–569 (1980).

Figures

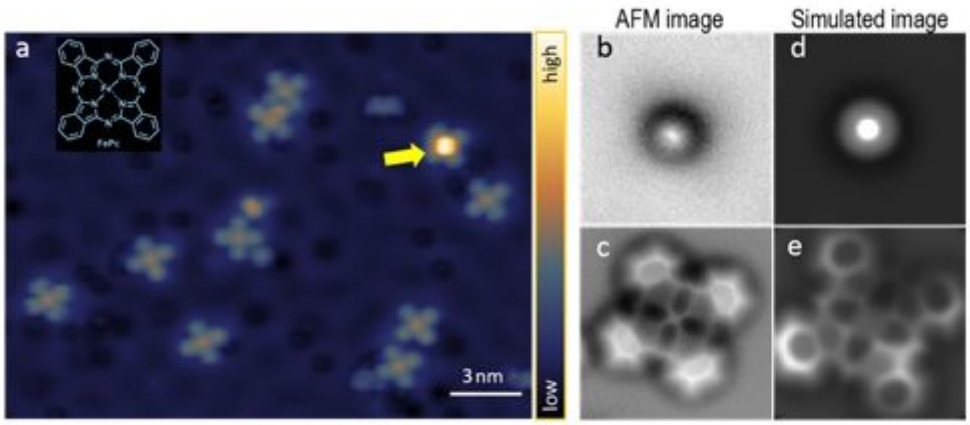

Figure 1

STM and AFM images of FePc and the datively bonded CO-FePc complex. a STM image of the FePc molecule with (indicated by the arrow) and without adsorption of CO, with the insert showing the chemical structure of FePc (set point: Vsample = +100 mV, I = 100 pA). b, c Experimental AFM images of FePc with and without adsorbed CO, obtained using a CO-terminated tip (V = 0 V, A = 100 pm) at tip heights Δz of -160pm and -10 pm, respectively. The tip height Δz was set with respect to a reference height ‘given by the STM set point (100 mV, 100 pA) above the bare Cu(111) substrate in the vicinity of the molecule. The minus sign indicates a relative tip height. d, e Simulated AFM images corresponding to CO-FePc and FePc.

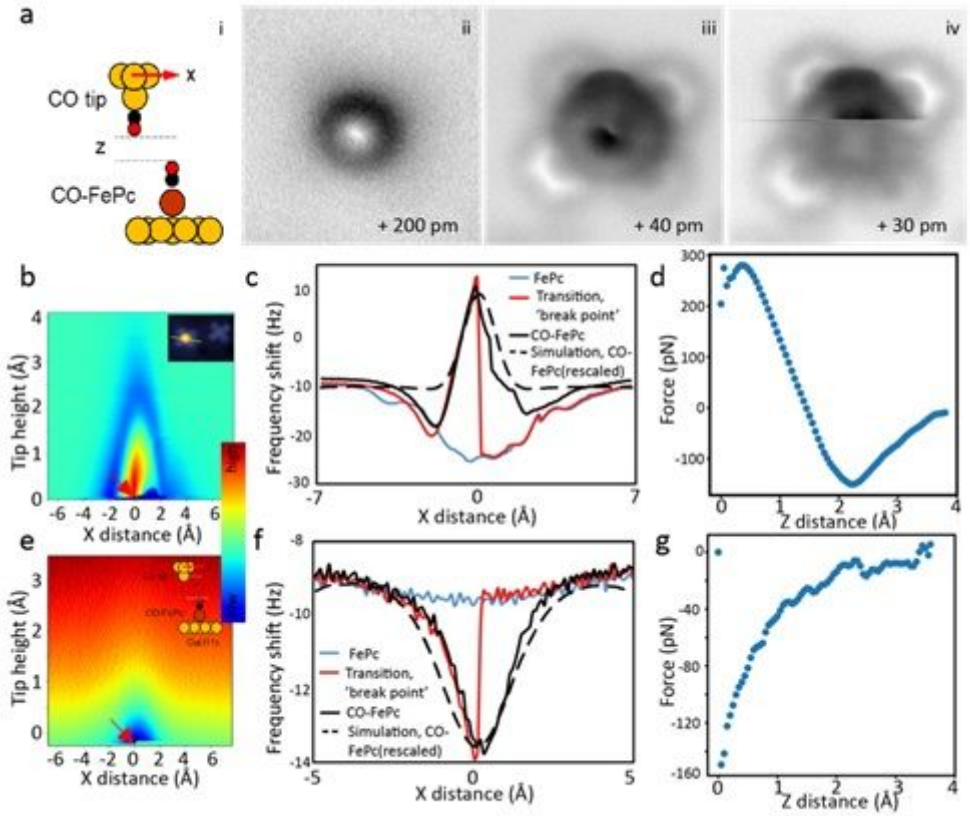

Figure 2

Rupturing the dative CO-FePc bond using AFM tips. a (i) Schematic of a CO-AFM tip interacting with CO-FePc (Cu: yellow; carbon: black; oxygen: red; Fe: orange) and (ii-iv) showing noncontact AFM images obtained at different tip heights (z) and the final dislodging of CO at z = +30 pm. b 3D force map of the frequency shift (Δf) vs. AFM tip heights (z) and horizontal position (x), with a CO tip. Step size is 5 pm in z, and the scan path in x is across the center of the Fe, as shown in the insert. The tip position at bond rupture is indicated by the break point (arrow). c Frequency shift (Δf) obtained in the horizontal (x) direction before, during (indicated by the disjointed curve), and after the bond rupture. d The force curve deconvoluted from Δf at the break point in the vertical (z) direction. e 3D force map of the frequency shift (Δf) showing quantitative rupture of the dative bond using a Cu tip; the insert shows schematic of interaction between a Cu tip and CO-FePc. f Frequency shift (Δf) obtained using a Cu tip scanned in the horizontal (x) direction. g The deconvoluted force curve at the break point in the vertical (z) direction using a Cu tip. (Red arrows indicate the bond rupture point, Long-range background forces are subtracted in Figures d and g).

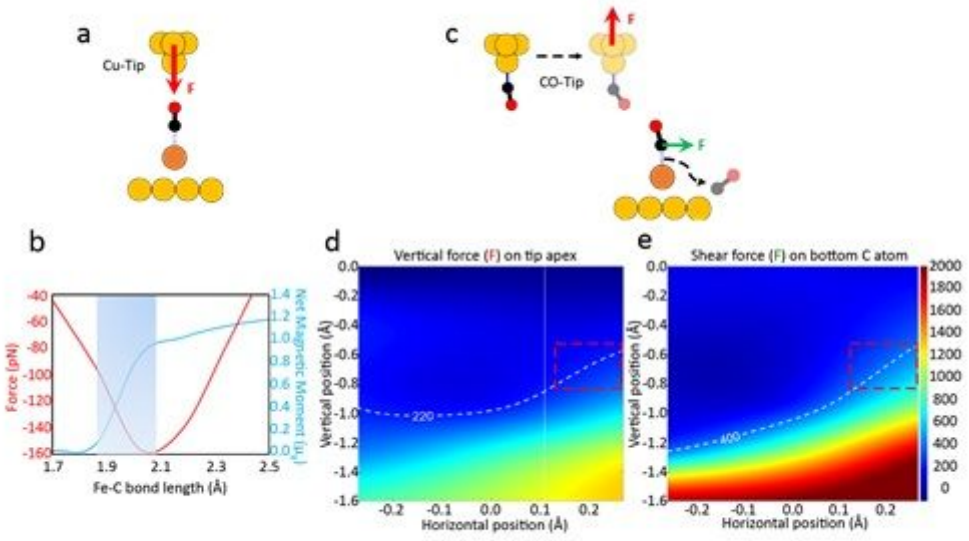

Figure 3

Real-space pseudo-potential DFT calculations for the breaking of the dative bond in CO-FePc. a Schematic showing the interaction of the Cu tip with the CO-FePc complex on Cu(111). b The red curve shows the calculated attractive vertical force on the Cu apex while the blue curve shows the net magnetic moment as a function of the Fe-C bond length. The shaded area indicates where the bond rupture process occurred. c Schematic shows the interactions between the CO-tip and the CO-FePc complex on Cu(111). d, e are contour plots for the calculated compressive vertical force on the tip apex, and the lateral force acting on the bottom C (of the CO attached to FePc). The x and y axes are the horizontal positions and heights of the tip with respect to an equilibrium position. The dashed curves in d and e correspond to the measured force, 220 pN, and where the shear force equals 400 pN. The red boxes indicate the same region in d and e. In a and c, the red and green arrows indicate the direction of the forces acting on the tip apex and on the bottom C atom, respectively.

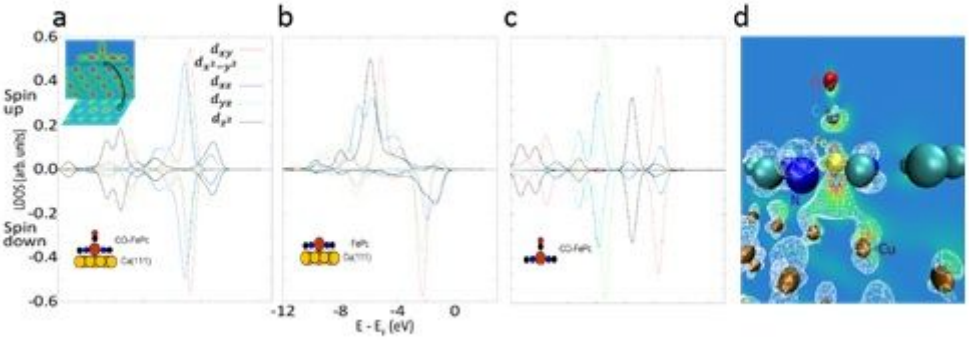

Figure 4

Spin-polarized LDOS projected onto the center Fe atom. a CO-FePc on Cu(111), b FePc on Cu(111), c CO-FePc without a substrate. In a, the top inset shows a 2D vertical profile of the total electron density across the Fe atom. The black arrow indicates a 2D horizontal profile in between the complex and the Cu surface where the red dashed rectangle encloses the two bridge Cu atoms underneath the center Fe. d The HOMO of the system (around the center Fe atom). A wireframe view of the orbitals is overlapped with a 2D vertical profile of the electron density. Isosurface value = 10-5 e/bohr3.

Supplementary Files

This is a list of supplementary files associated with this preprint. Click to download.

- BreakingaDativeBondwithMechanicalForcesChenetalSupplementaryMaterials2021.docx